Journal of Biomolecular NMR, **16:** 9–21, 2000.
KLUWER/ESCOM

Assessment of zinc finger orientations by residual dipolar coupling constants

Vickie Tsui, Leiming Zhu*, Tai-Huang Huang**, Peter E. Wright*** & David A. Case***
Department of Molecular Biology, The Scripps Research Institute, La Jolla, CA 92037, U.S.A.

Received 20 August 1999; Accepted 27 October 1999

Key words: dipolar couplings, domain orientation, transcription factor III A, zinc fingers

Abstract

Residual dipolar coupling constants measured in anisotropic solution contain information on orientations between internuclear vectors and the magnetic field, providing long-range information that may help determine the relative orientations of distinct domains in biomolecules. Here we describe the measurement and use of residual dipolar coupling restraints in the refinement of the structure of the complex of DNA with three zinc fingers of transcription factor IIIA (TFIIIA), measured in a DMPC/DHPC bicelle solution. These dipolar restraints were applied on a variety of orientations of the zinc finger domains (derived from crystallography, previous NMR studies, and systematic modeling) in order to examine the validity and sensitivity of using residual dipolar splittings to study interdomain orientations. The spread in interdomain angles between zinc fingers is reduced from 24° to 9° upon incorporation of dipolar restraints. However, the results also show that the ability to determine relative orientations is strongly dependent on the structural accuracy of the local domain structures.

Introduction

Nuclear magnetic resonance spectroscopy has emerged as a major tool in structure determination of biomolecules. Its abilities to examine structures in aqueous solution, probe the dynamics of the system, and study the behavior of bound water molecules give the technique several advantages over X-ray crystallography. Nevertheless, there are limitations stemming from the inherent nature of structural information provided by NMR data. The conventional approach to NMR structure determination involves the conversion of nuclear Overhauser effects (NOEs) to proton-proton distances as restraints in structure calculations. NOEs can only be observed for pairs of nuclei that are within about 5 Å of each other, so that the structural information is short-ranged (Clore and Gronenborn, 1998). The lack of long-range experimental restraints may lead to uncertainties in structure determination when the system contains distinct domains, whose interactions with each other and positioning with respect to one another may not be accurately described by the small number of observable short-ranged NOEs.

A new technique was introduced recently that can improve the accuracy of NMR structure determination by directly measuring internuclear dipolar coupling constants in biomolecules (Tjandra and Bax, 1997; Prestegard, 1998). The introduction of anisotropy using dilute solutions of magnetically oriented particles, such as bicelles, yields a small degree of solute alignment, leading to readily measurable residual dipolar splittings between pairs of nuclei. The magnitude of the dipolar splitting is related to the angle between the corresponding internuclear vector and the direction of the magnetic field, B_o. Because the direction of B_o is fixed over the entire molecule, angles made with respect to B_o in turn relate the orientations of the internuclear vectors to each other, independent of the distance between the vectors. Therefore, dipolar coupling constants have the potential of providing

*Present address: Monsanto Co., BB4I, 700 Chesterfield Parkway, St. Louis, MO 63198, U.S.A.
**Present address: Institute of Biomedical Sciences, Academica Sinica, Tapei, Taiwan.
***To whom correspondence should be addressed.

important long-range information for NMR structure determination.

Since the introduction of this method, there have been several efforts to examine the usefulness of such data and to apply them to structure refinement (Tjandra et al., 1997; Banci et al., 1998; Ottiger et al., 1998b; Clore et al., 1999; Fischer et al., 1999). The relative positioning of protein domains could in principle be determined by dipolar coupling data. For a correctly determined structure with fixed relative interdomain orientation, the different domains should have a common alignment tensor. Thus, knowing the substructures of the domains, one should be able to determine the relative orientations of the domains (Prestegard, 1998; Fischer et al., 1999; Losonczi et al., 1999).

To test this idea, we used a system of three zinc fingers of transcription factor IIIA (TFIIIA) bound to the cognate DNA. Each zinc finger is a compact globular domain containing an α-helix and a small β-sheet. Zinc finger 1 consists of residues 12 to 37, zinc finger 2 consists of residues 42 to 67, and zinc finger 3 consists of residues 72 to 98, using the numbering scheme in the NMR and crystal structures. These residues comprise the core region of the zinc finger domains. The fingers are connected by flexible polypeptide linkers and display rigid-body motions in the absence of DNA (Brüschweiler et al., 1995). When bound to DNA, the domains become ordered, and the linkers lose their intrinsic flexibility (Foster et al., 1997). The NMR solution structure of this complex was recently solved by conventional methods (Foster et al., 1997; Wuttke et al., 1997) and was followed by a 3.1 Å crystal structure of the complex of six zinc fingers of TFIIIA bound to DNA (Nolte et al., 1998). Comparison of the NMR and crystal structures shows generally close agreement in the local zinc finger conformations and DNA contacts, but there is a noticeable difference in the relative positioning of the first and second amino-terminal zinc fingers. In the NMR structure, these two fingers are closely packed, with a significant protein–protein interface formed between them. The relative orientation of these fingers differs in the crystal structure, such that there are fewer packing contacts between them. Here we report the use of dipolar coupling constants to examine the relative orientation between the first two zinc finger domains. We have carried out structure refinement using a combination of NOE, J-coupling and dipolar coupling data, and have applied dipolar restraints directly to the previously obtained structures in order to study the effects of domain substructure on orientational preference. We will discuss the potential as well as limitations of this method.

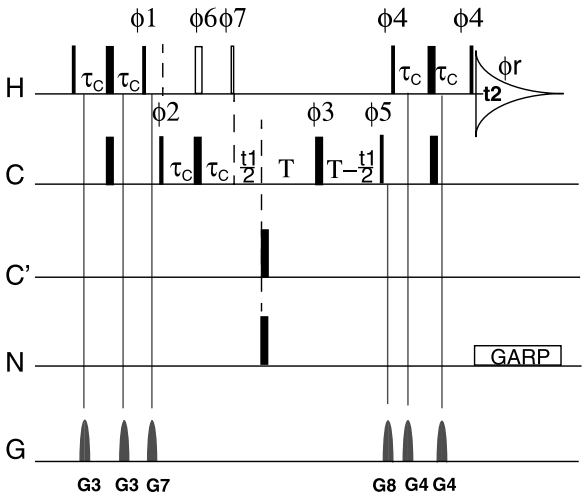

Figure 1. The pulse sequence of IPAP-CT-C13 HSQC. Narrow rectangular pulses represent 90° flip angle pulses, and wider ones 180° flip angle pulses. $180^\circ_{\phi 6}$ and $90^\circ_{\phi 7}$ are only used for AP FIDs, but not for IP FIDs. The IP and AP FIDs are acquired in an interleaved fashion. Cα (and CO) 90° and 180° pulse widths were adjusted so that the excitation profile had a null CO (and Cα); i.e. $pw(90) = \sqrt{15}/4\delta$, $pw(180) = \sqrt{3}/2\delta$, where δ is the frequency difference between Cα region and CO region. The phases are along +x unless otherwise indicated. ϕ1 = y,−y; ϕ2 = x,x,−x,−x; ϕ3 = 4(x), 4(y), 4(−x), 4(−y); ϕ4 = 16(x), 16(y); ϕ7 = 16(x),16(−x); ϕr = 2(x,−x,−x,x,−x,x,x,−x),2(−y,y,y,−y,y,−y,−y,y); ϕ5 = x + δϕ5, δϕ5 = −52°, resulting from the CO 180° off-resonance effect during the t_1 evolution (Cavanagh et al., 1996).

Methods

Experimental procedures

A 20% DMPC/DHPC bicelle stock solution with an approximate molar ratio of 3:1 was added to the protein samples, so that a 4–5.5% final bicelle solution was obtained. The solution was titrated with either 20% DMPC or DHPC to obtain a stable, aligned bicelle medium, as judged by the splitting of the ^{2}H resonance in D_2O. The residual dipolar couplings were obtained by subtracting the isotropic ^{1}J(N-H) and ^{1}J(Cα-Hα) coupling constants measured in the absence of bicelles, from the D+J values measured using the aligned bicelle medium. All measurements were made at 37 °C.

The N-H dipolar splittings were measured with ^{15}N-labeled samples using the pulse sequence of Ottiger et al. (1998a). Sixteen scans were used in both the J measurement (in isotropic solution) and the J+D

measurement (in the aligned medium). The spectral width and acquisition time were 8992.8 Hz (centered at 4.7 ppm) and 114 ms, respectively, in the t_2 (^{1}H) dimension. In the t_1 (^{15}N) dimension, these values were 2356.6 Hz (centered at 118 ppm) and 109 ms, respectively. Further zero-filling and application of appropriate window functions (Gaussian broadening (6 Hz)/exponential narrowing (6 Hz) in ^{1}H, and a 90°-shifted sinebell function in the ^{15}N dimension) resulted in a final matrix of dimension 1024 × 1024.

The Cα-Hα dipolar splittings were measured on a ^{15}N, ^{13}C-labeled sample in D_2O buffer using an IPAP-CT-HSQC experiment, as shown in Figure 1. In Figure 1, $180^\circ_{\phi 6}$ and $90^\circ_{\phi 7}$ were only used in the AP experiment, but not in the IP experiment. Cα (and CO) 90° and 180° pulse widths were adjusted so that the excitation profile had a null at CO (and Cα); i.e. $pw(90) = \sqrt{15}/4\delta$ and $pw(180) = \sqrt{3}/2\delta$, where δ is the frequency difference between the Cα region and the CO region (Cavanagh et al., 1996). $90^\circ_{\phi 5}$ was corrected for 52° to compensate for the CO 180° off-resonance effect (Cavanagh et al., 1996). In both the J measurement (in isotropic solution) and J+D measurement (in the aligned medium), 128 scans were used. The spectral width and acquisition time were 4960 Hz (centered at 3 ppm) and 103 ms in t_2 (^{1}H dimension), respectively. In t_1 (^{13}C dimension), these values were 7.15 kHz (centered at 50 ppm) and 22.4 ms, respectively. Data in the ^{13}C dimension was linear-predicted to 44.8 ms (i.e. from 160 to 320 complex points). After zero-filling and application of appropriate window functions (Gaussian broadening (6 Hz)/exponential narrowing (6 Hz) in ^{1}H and 90°-shifted sinebell-squared function in the ^{13}C dimension), a final matrix of dimension 512 × 2048 was obtained. Figure 2 shows regions of (A) upfield and (B) downfield doublet components of a [^{13}C, ^{1}H] IPAP-CT-HSQC experiment on the TFIIIA/DNA complex.

Two sets of dipolar coupling constants were obtained for ^{13}Cα-^{1}H from a double-labeled sample at around 5.5% bicelle concentration in D_2O buffer. These data were averaged to give the values used as restraints, giving 60 data points. The average unsigned deviation between these two sets of data was 0.5 Hz. Two sets of dipolar coupling constants were obtained for ^{15}N-^{1}H using two ^{15}N-labeled samples at bicelle concentrations of 4% and 5.5% in 10% D_2O:90% H_2O buffer. Figure 3 shows a comparison of these data. With the exception of one dipolar splitting, that of a histidine residue in zinc finger 2, the two sets of data were simple multiples of each other. The set of data obtained at 5.5% bicelle concentration was used because this concentration was closer to the concentration at which the ^{13}Cα-^{1}H data were obtained. The dipolar splittings for the different sets of ^{15}N-^{1}H and ^{13}Cα-^{1}H data are given in Table 1.

Refinement using residual dipolar couplings

All simulations were performed using AMBER 5 (Case et al., 1997), which has been modified to incorporate residual dipolar coupling restraints; the modifications are included in AMBER 6. Following the notation of Bastiaan et al. (1987), the residual dipolar coupling between a pair of spin 1/2 nuclei, *i* and *j*, can be written as

$$D = \frac{\mu_0}{4\pi}\frac{\gamma_i\gamma_j h}{2\pi^2 r^3}\left\langle P_2(\hat{z}' \cdot \hat{z}'')\right\rangle \quad (1)$$

where μ_0 is the magnetic permeability of vacuum, γ_i and γ_j are gyromagnetic ratios, *h* is Planck's constant, *r* is the distance between *i* and *j*, $\hat{z}'$ is a unit vector along the direction of the magnetic field, and $\hat{z}''$ is a unit vector along the internuclear axis. The brackets indicate averaging in the presence of internal motion and tumbling. In isotropic solution, this term averages to zero. Anisotropy in the solution induces slight alignment preferences in the tumbling molecule and gives rise to measurable values of *D*.

Equation 1 can be rearranged to refer to an overall molecular frame, denoted by unprimed variables $\hat{p}$, $\hat{q} = (\hat{x}, \hat{y}, \hat{z})$ (Bastiaan et al., 1987):

$$\begin{aligned} D &= \frac{\mu_0}{4\pi}\frac{\gamma_i\gamma_j h}{2\pi^2 r^3}\sum_{p,q}\left\langle\frac{3}{2}(\hat{p}\cdot\hat{z}') - \frac{1}{2}\delta_{pq}\right\rangle \\ &\quad \left\langle\frac{3}{2}(\hat{p}\cdot\hat{z}'')(\hat{q}\cdot\hat{z}'') - \frac{1}{2}\delta_{pq}\right\rangle \\ &\equiv -\frac{\mu_0}{4\pi}\frac{\gamma_i\gamma_j h}{2\pi^2 r^3}\sum_{p,q} A_{pq}\Gamma_{pq} \end{aligned} \quad (2)$$

The expression for the dipolar coupling constant is thus broken down into two parts: **A** is the Saupe order matrix and carries out the transformation from the laboratory frame to the molecular frame, and Γ carries out the transformation from the molecular frame to the local frame of the individual vectors. Γ depends only on the molecular structure and relates each spin–spin vector to the molecular coordinate frame. In the case that the internal motion of a bond vector is cylindrically symmetric about its average position, Γ can be expressed in terms of the average bond vector $\hat{z}^{av}$ (see Appendix):

Table 1. Experimental dipolar splittings for backbone ^{15}N-^{1}H and ^{13}Cα-^{1}H of the three N-terminal zinc fingers of Transcription Factor IIIA (TFIIIA) when bound to DNA

A. ^{15}N-^{1}H Dipolar coupling constants

Res	Conc. 1[a]	Conc. 2[b]	Res	Conc. 1[a]	Conc. 2[b]	Res	Conc. 1[a]	Conc. 2[b]
Arg12	−2.22	−4.76	Cys45	6.21	14.52	Cys75	0.66	2.19
Tyr13	−5.77	−12.15	Lys46	−0.24	−0.01	Asp76	−1.21	−2.34
Thr14	−5.88	−12.69	Glu47	8.24	19.44	Ser77	−0.73	−0.77
Cys15	0.60	1.32	Glu48	3.53	8.18	Asp78	6.15	13.67
Phe17	−5.51	−12.17	Gly49	−8.58	−17.06	Gly79	3.92	10.52
Ala18	2.97	6.25	Cys50	5.67	12.80	CYS80	0.26	1.48
Asp19	−2.84	−4.76	Glu51	−0.85	−0.88	Asp81	−1.38	−2.96
Cys20	−2.35	−4.42	Lys52	−1.94	−3.19	Leu82	5.31	12.8
Gly21	−1.94	−2.20	Gly53	6.70	16.30	Arg83	1.23	3.89
Ala22	2.58	6.07	Phe54	7.49	17.18	Phe84	1.64	5.91
Ala23	−2.30	−4.40	Thr55	−3.48	−5.05	Thr85	4.01	9.85
Tyr24	−5.78	−11.85	Ser56	5.60	–	Thr86	−2.90	−4.67
Lys26	0.52	2.34	Leu57	−5.36	−11.20	Lys87	−5.74	−11.21
Asn27	0.92	2.49	Leu60	−6.22	−13.48	Ala88	−5.34	−10.87
Trp28	1.71	4.02	Thr61	−4.19	−7.62	Asn89	3.63	8.86
Lys29	−0.69	−0.34	Arg62	−5.77	−11.66	Met90	−2.50	−4.47
Leu30	0.87	2.55	His63	−14.70	−20.21	Lys91	−5.73	−11.38
Gln31	1.16	3.74	Ser64	−4.59	−9.22	Lys92	−0.33	0.26
Ala32	1.95	5.38	Leu65	1.85	5.41	His93	2.55	5.15
His33	−0.17	0.93	Thr66	−9.80	−19.59	Phe94	−3.34	−6.76
Leu34	1.48	4.77	His67	−4.21	−7.64	Asn95	−7.00	−13.65
Ser35	−0.11	0.28	Thr68	0.54	3.75	Arg96	3.79	9.23
His37	1.64	4.94	Gly69	−3.69	−6.47	Phe97	−0.78	−3.77
Thr38	−0.70	−0.04	Glu70	−8.37	−17.78	His98	−10.37	−21.82
Gly39	3.61	9.27	Lys71	0.72	1.74	Asn99	−0.51	−0.32
Glu40	−0.30	−0.71	Asn72	−7.54	−15.49	Ile100	1.24	3.48
Lys41	3.48	8.01	Phe73	1.05	2.89	Lys101	1.05	2.74
Phe43	7.54	18.04	Thr74	1.32	4.18			

B. ^{13}Cα−^{1}H Dipolar coupling constants

Res	<D>[c]	dD/2[d]	Res	<D>[c]	dD/2[d]	Res	<D>[c]	dD/2[d]
Met1	7.32	0.35	Phe43	14.49	1.54	Thr74	4.83	0.39
Tyr13	−23.29	1.09	Pro44	15.54	0.07	Asp76	20.07	1.80
Ile14	−21.60	1.45	Cys45	2.71	1.01	Ser77	13.45	0.30
Ser16	11.6	0.50	Glu47	23.01	0.26	Asp78	11.64	0.21
Ala18	−3.83	0.15	Cys50	−2.93	0.03	Cys80	−6.10	0.31
Asp19	16.73	0.09	Phe54	18.53	0.77	Asp81	2.44	0.40
Cys20	−10.75	0.16	Thr55	−15.70	0.15	Leu82	19.51	0.13
Ala22	6.24	0.12	Ser56	−26.10	1.73	Arg83	9.49	0.47
Ala23	2.75	0.31	Leu57	13.60	0.14	Phe84	6.04	0.12
Tyr24	−10.40	0.57	Leu60	3.72	1.32	Thr85	25.86	0.10
Asn25	−28.04	1.74	His63	−2.20	0.75	Lys87	−27.31	0.71
Lys26	−8.13	0.50	Ser64	4.24	0.01	Ala88	7.88	0.04
Asn27	1.89	0.03	Leu65	19.39	0.40	Asn89	21.81	0.09
Lys29	−16.24	0.32	Thr66	−23.21	0.81	His93	7.36	0.97
Ala32	22.62	0.17	His67	0.63	1.69	Phe94	−21.88	2.37
Ser35	−3.58	0.07	Thr68	24.09	0.51	Asn95	−4.44	0.58
His37	9.60	0.88	Glu70	−15.65	0.77	His98	−29.37	0.32
Glu40	15.08	1.69	Lys71	−9.67	0.53	Asn99	−3.40	0.21
Lys41	20.44	0.75	Asn72	2.74	0.59	Ile100	2.36	0.11
Pro42	−8.95	0.31	Phe73	5.86	0.27	Lys101	−0.14	0.16

[a]Measured in 4% bicelle, q = DMPC/DHPC = 3.0.
[b]Measured in 5.5% bicelle, q = DMPC/DHPC = 3.0.
[c]Average dipolar splitting from two sets of data measured at 5.5% bicelle, q = DMPC/DHPC = 3.0.
[d]Average error between two sets of data.

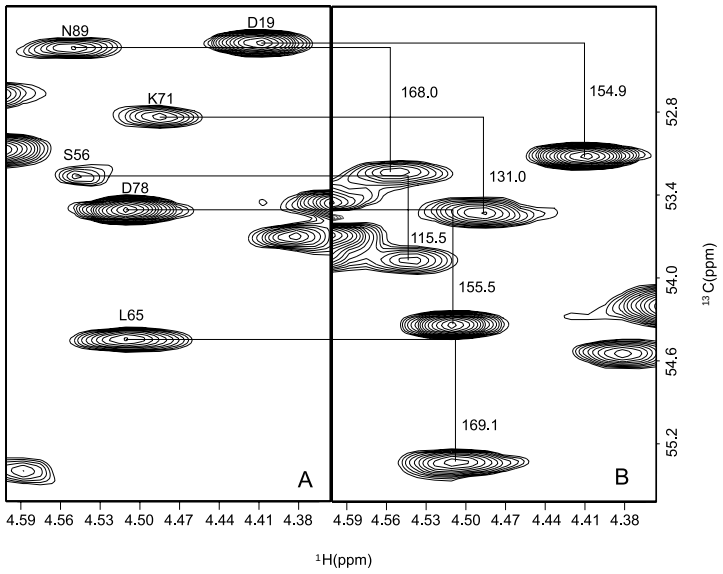

Figure 2. Regions of the TFIIIA/DNA complex [^{13}C, ^{1}H] IPAP-CT-HSQC spectrum. (A) Upfield and (B) downfield doublet components. Experimental conditions are described in the text.

$$\Gamma_{pq} = S\left\langle \frac{3}{2}(\hat{p}\cdot\hat{z}^{av})(\hat{q}\cdot\hat{z}^{av}) - \frac{1}{2}\delta_{pq}\right\rangle \qquad (3)$$

where S is the order parameter introduced by Lipari and Szabo (Lipari and Szabo, 1982). The alignment tensor **A** is a symmetric, traceless tensor with five variable parameters (Bastiaan et al., 1987; Bothner-By, 1996), which we take as *Ayy*, *Azz*, *Axy*, *Axz* and *Ayz*. This is an alternative to models that consider the axial and rhombic components, plus the three Euler angles, as variable parameters. Expanded into individual terms, the equation for the dipolar coupling constants becomes

$$\begin{aligned} D \;=\; & \frac{\mu_0}{4\pi}\frac{\gamma_i\gamma_j h}{2\pi^2 r^3} S[\cos^2\phi_x(-A_{yy}-A_{zz}) \\ & +\cos^2\phi_y A_{yy} + \cos^2\phi_z A_{zz} \\ & +2\cos\phi_x\cos\phi_y A_{xy} \\ & +2\cos\phi_x\cos\phi_z A_{xz} \\ & +2\cos\phi_y\cos\phi_z A_{yz}] \end{aligned} \qquad (4)$$

where $\cos\phi_i$ is the projection of the average internuclear vector onto axis i. Differentiation of Equation 4 with respect to atomic coordinates or elements of the **A** tensor is straightforward; the use of Cartesian components as parameters simplifies the expressions for derivatives and avoids singularities as special Euler angles.

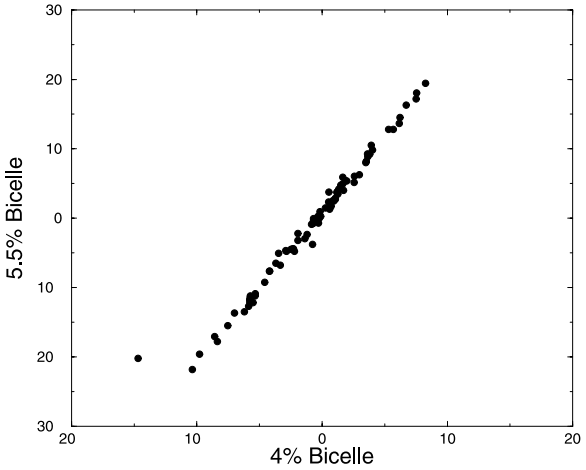

Figure 3. Plot of ^{15}N-^{1}H dipolar splittings obtained at bicelle concentrations of 5.5% versus 4%. The splittings are expressed in units of Hz. The outlier point at the lower left is for residue His 63.

To find the optimal alignment tensor for a fixed structure, given a set of experimental dipolar couplings, AMBER optimizes the five parameters in **A** by minimizing the energy term

$$E_{dipolar} = k_{dipolar}(D_{calc} - D_{\exp})^2 \qquad (5)$$

where $k_{dipolar}$ is a force constant. For a fixed structure, the optimal **A** tensor can be determined by minimizing $E_{dipolar}$, and one can use $\mathbf{A} \equiv 0$ (the isotropic case) as a starting guess. In a structure refinement, where the atomic coordinates and the **A** matrix are simul-

taneously optimized, the total energy of the system includes $E_{dipolar}$, the force field energy terms, and energy terms from any other NMR restraints, such as distance or torsion angle restraints. The structure is continuously adjusted to both satisfy experimental data and maintain low force field energy, while the alignment tensor is continuously adjusted to fit the current structure.

Simulated annealing refinement

Each of the 22 original NMR structures (Wuttke et al., 1997) [Brookhaven PDB 1TF3] and the relevant portion of the X-ray structure [PDB entry 1TF6] was subjected to a round of simulated annealing, heating to 400 K and cooling to 0 K over a total of 15 ps. The structures were refined against residual dipolar coupling restraints and the distance and dihedral angle restraints used to determine the original NMR structures (Wuttke et al., 1997). These include 1819 distance restraints derived from intermolecular and intramolecular NOEs, as well as torsional restraints for 54 backbone ϕ and 60 side-chain χ^1 dihedral angles derived from three-bond homonuclear and heteronuclear coupling constants. Additional restraints for ω dihedral angles, chirality, Watson–Crick hydrogen-bonding, and DNA phosphate backbone torsional angles were also included, as described previously (Wuttke et al., 1997).

When dipolar coupling restraints are included, we have found it necessary to increase angle and torsion force constants to prevent violations of local geometries. To prevent such structural distortions, the force constant for the NMR-based torsion angle restraints was increased from 32 kcal mol^{-1} rad^{-2} to 300 kcal mol^{-1} rad^{-2}. For the same reason, we also added angle restraints to maintain ideal backbone geometry. The Hα-Cα-Cβ, Hα-Cα-N, and Hα-Cα-C angles were restrained to 109.5°, and the H-N-C and H-N-Cα angles were restrained to 119° with a force constant of 1000 kcal mol^{-1} rad^{-2}. Different trials were conducted to find a force constant for the dipolar restraints large enough to give good agreement between experimental and calculated dipolar coupling splittings, and still not introduce serious violations in the other restraints. Two sets of simulations will be described, one with a force constant of 1.0 kcal mol^{-1} Hz^{-2}, and one with a force constant of 0.3 kcal mol^{-1} Hz^{-2}. (In principle, a different force constant should be used for N-H and C-H couplings to reflect the different γ values, but this was not done here.) The structures with the weaker force constant turned out to satisfy the dipolar coupling restraints to within the estimated experimental errors (see below), and will be referred to as the 'joint refinement results', since they were determined with conventional and dipolar coupling restraints active simultaneously.

This joint refinement (using both conventional and dipolar restraints) has the advantage of using all available information, but suffers the disadvantage that it could fail to detect incorrect alignments (e.g. that could result from errors in the NOE assignments), and does not use the dipolar restraints in an independent way to assess the correctness of the finger–finger alignment. To see if our results might be biased toward the original NMR family, one of the original NMR structures was subjected to two additional rounds of simulated annealing refinement, using the same protocols as above, but with a reduced set of restraints that excluded all NOE restraints between zinc fingers 1 and 2. The first round included only dipolar coupling restraints in the core region of zinc finger 1 (residues 12 to 37), whereas the second round used only dipolar coupling restraints in the core region of zinc finger 2 (residues 42 to 67). These 'individually refined' local zinc finger structures were used in the analysis described below, and the results compared to those obtained when all NMR restraints were included in the calculation.

Results and discussion

Treatment of the residual dipolar coupling data

As described in the Methods section, the two sets of ^{15}N-^{1}H dipolar couplings obtained at different bicelle concentrations were simple multiples of each other. Thus, it is likely that, for our ^{15}N-^{1}H and ^{13}Cα-^{1}H data, which differ slightly in bicelle concentration, the alignment tensors maintain the same tensor direction and differ only in magnitude. To determine the optimal scaling, simulated annealing calculations were performed using independent alignment tensors for the two sets of data (^{15}N-^{1}H and ^{13}Cα-^{1}H), thus optimizing 10 alignment parameters. This produced final structures with alignment tensors that are similar to each other in direction (within 12°) and magnitude ($A_{CH,calc}/A_{NH,calc} = 0.9$, where A is one of the principal components of the alignment tensor). To minimize the effect of incorrect structures on the fitting of alignment tensors, and to make sure the treatment of residual dipolar coupling data is not biased towards the domain orientations of the original NMR

Table 2. Summary of structural statistics[a]

	Original NMR refinement	With strong dipolar rst[c]	With weak dipolar rst[c]
Average unsigned deviation from distance restraints[b] (Å)	0.0036	0.0047	0.0046
Average unsigned deviation from dihedral restraints[b] (°)	0.058	0.026	0.025
Average unsigned deviation from dipolar restraints[d] (Hz)			
Overall	4.62	0.25	0.71
ZF1	3.25	0.24	0.65
ZF2	3.99	0.23	0.72
ZF3	3.68	0.22	0.64
AMBER energy (kcal mol^{-1})	−2546	−2389	−2421
Deviation from ideal bonds (Å)	0.0054	0.0031	0.0036
Deviation from ideal torsion angles (°)	2.6	1.4	1.2

[a]Statistics were averaged over ensembles of 22 structures for each family of structures.
[b]None of the distance violations exceeded 0.4 Å, and none of the dihedral angle violations exceeded 7°.
[c]Strong: force constant = 1.0 kcal mol^{-1} Hz^{-2}; weak: force constant = 0.3 kcal mol^{-1} Hz^{-2}.
[d]For the crystal structure, the average unsigned deviations from dipolar restraints are 4.31 Hz overall, 2.16 Hz for ZF1, 4.94 Hz for ZF2, and 3.78 Hz for ZF3.

Table 3. Root-mean-square deviations from mean structures[a]

	Rmsd when fitting all[b] (Å)	Rmsd when fitting zf2[c] (Å)
Original	0.63	1.21
Strong dipolar[d]	0.39	0.58
Weak dipolar[d]	0.40	0.67

[a]The rmsd values were calculated for backbone heavy atoms (Cα,N,C,O) of residues 12–98, containing all three zinc fingers and linker regions.
[b]Structures were superimposed on backbone heavy atoms of residues 12–98.
[c]Structures were superimposed on backbone heavy atoms of residues 42–67 (zinc finger 2 without linker regions).
[d]Strong: force constant = 1.0 kcal mol^{-1} Hz^{-2}; weak: force constant = 0.3 kcal mol^{-1} Hz^{-2}.

structures, only the third zinc finger in the original NMR structures, which gave the best results, was used in the following procedure. For this zinc finger, 8 out of 11 structures whose tensor directions for the two sets of data were within 10° gave $A_{CH,calc}/A_{NH,calc} = 0.9$. This is consistent with the ratio obtained from the set of simulated annealed structures. Therefore, a scaling factor of 0.9 was introduced for the ^{15}N-^{1}H data, and only a single tensor was optimized for the rest of the simulations. This reduced the number of fitting parameters from 10 to 5.

As shown in the Appendix, dipolar coupling constants are dependent on S, the square root of the order parameter S^2. In our calculations, the dipolar coupling values for only the 54 residues with $S^2 \geq 0.80$ were used, where S^2 values were determined from ^{15}N relaxation studies (Radhakrishnan and Wright, unpublished data). Over these 54 residues, values of S ranged from 0.89 to 0.98. Assuming a common value should introduce little error, a uniform S value of 1 was used.

Results of simulated annealing

As described in the Methods section, two sets of dipolar-refined structures were determined, with force constants for dipolar coupling restraints set to 1.0 kcal mol^{-1} Hz^{-2} and 0.3 kcal mol^{-1} Hz^{-2}. The refinement starting from the crystal structure is also included in the family refined with weaker dipolar constraints. Table 2 provides a summary of the statistics of three families of structures: the original solution structures refined without dipolar restraints (Wuttke et al., 1997), and the two sets of structures refined with different weights on the dipolar restraints. The dipolar coupling refined structures show dramatic improvement in the agreement between experimental and calculated dipolar coupling data, even with the smaller

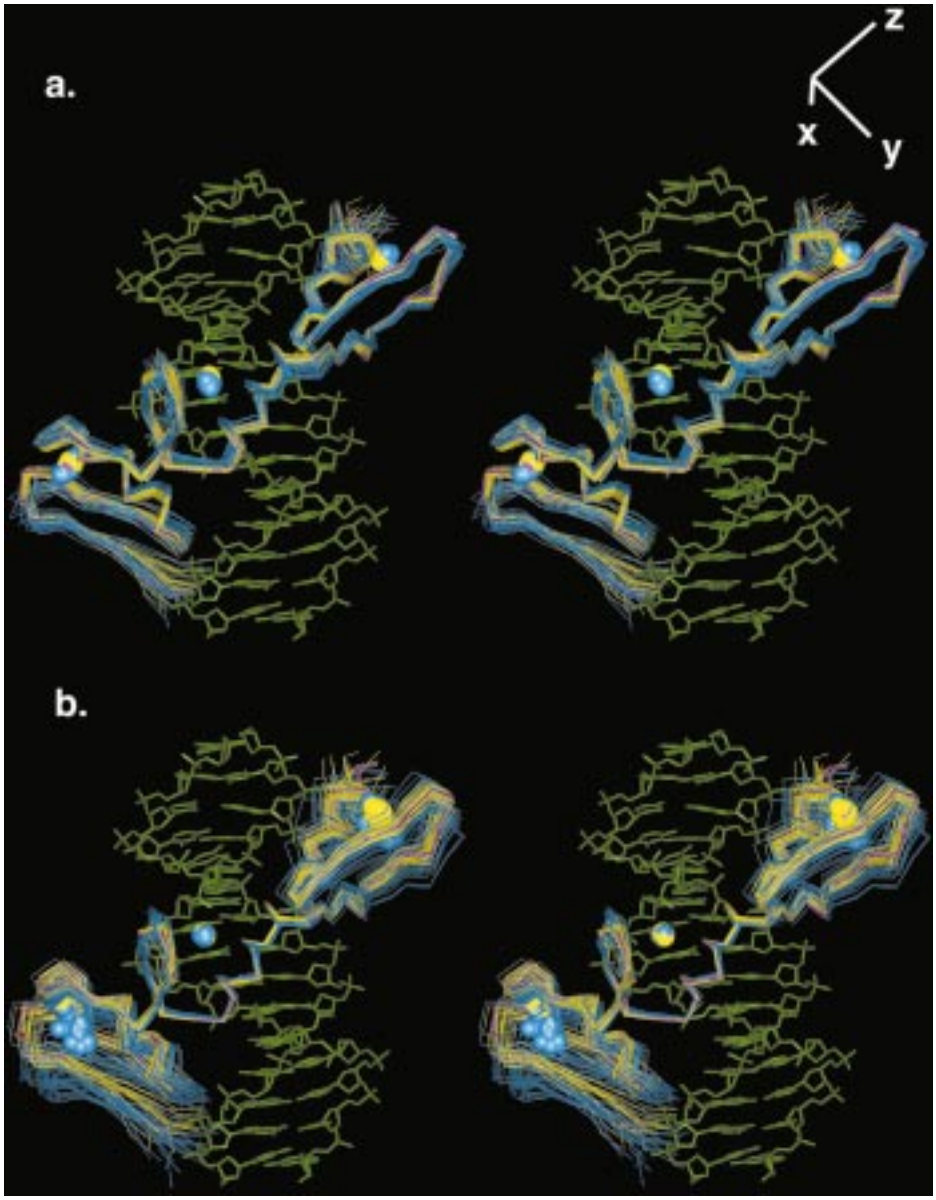

Figure 4. Stereo plots showing the backbone of the protein and the features of the DNA for the two ensembles of structures, refined with and without dipolar coupling restraints. Cyan: without dipolar restraints. Yellow: with dipolar restraints at a force constant of 0.3 kcal mol^{-1} Hz^{-2}. Red: crystal structure refined with NOE and dipolar restraints. (a) Structures were superimposed on all protein backbone heavy atoms (Cα, N, C, O of residues 12 to 98). (b) Structures were superimposed on backbone heavy atoms of the second zinc finger domain, residues 42–67. The coordinate frame of the alignment tensor is shown above, with the z axis representing the direction of the axial component of the tensor.

force constant. The two sets of dipolar-refined structures were similar, with an rmsd for all heavy atoms of 0.18 Å between their mean structures. The mean difference between calculated and fit dipolar couplings for the strong and weak dipolar restraints (0.25 and 0.71 Hz) straddle the estimated experimental uncertainty of 0.5 Hz, as measured by the reproducibility of repeated experiments (see above). The rmsd for all heavy atoms between the mean structure of the original family and those of the two dipolar-refined families was 0.43 and 0.42 Å for the stronger and weaker weights on dipolar restraints, respectively; this shift of mean structure is smaller than the spread of the earlier structures about their mean (0.92 Å for all

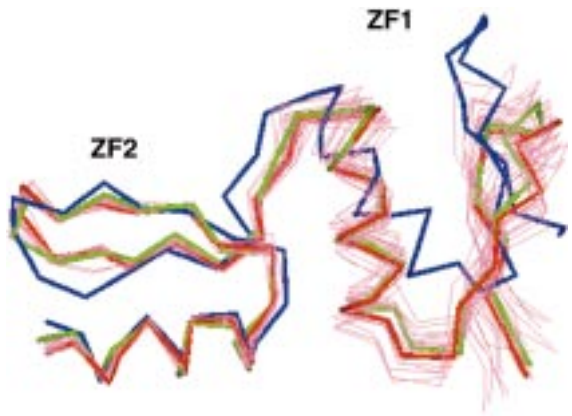

Figure 5. Variations in zinc finger 1 upon superposition of the zinc finger 2 backbone Cα atoms. Red: original NMR structure. Blue: crystal structure. Green: dipolar refined structure. The original NMR structure and dipolar refined structure are taken from the structure in the family closest to the mean. The family of original NMR structures is also shown as light red lines to indicate the amount of variation in the ensemble.

heavy atoms). However, the families of dipolar-refined structures were generally tighter, with increased overall precision (see Table 3). Especially interesting is the comparison between rmsd values of the protein backbone heavy atoms when the families of structures were superimposed on the backbone heavy atoms of the core region of zinc finger 2 (residues 42 to 67). These values indicate the tightness of the ensemble in terms of relative positioning between different zinc fingers, and show that the domain orientation becomes better defined with the addition of dipolar restraints. This tightening of structural families is illustrated in Figure 4. Figure 4a shows the original structures and the structures refined with lighter weights on dipolar restraints, when superimposed on all protein backbone heavy atoms. The difference in precision between the two families becomes clearer in Figure 4b, where the same two ensembles of structures were superimposed on the backbone heavy atoms of the second zinc finger only (residues 42 to 67). Zinc fingers 1 and 3 are more poorly superimposed in the original structures, taking up a larger range of orientations due to uncertainties in finger–finger packing. These two fingers are more well defined in the family of dipolar-refined structures. The refinement starting with the crystal structure is also depicted in Figure 4 (red). These show that the combination of NOE and dipolar coupling restraints was able to arrive at a common family of structures, even from a significantly different starting conformation.

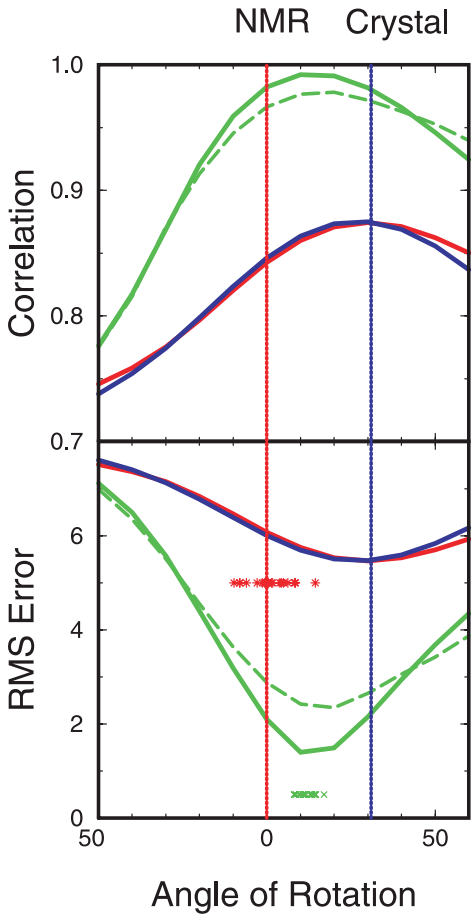

Figure 6. Plot of correlation coefficient and rms error between calculated and experimental dipolar coupling data for zinc fingers 1 and 2 at various angles of rotation of finger 1 about an axis that relates the NMR and crystal orientations to each other directly. The NMR and crystal orientations are marked by red and blue dotted vertical lines, respectively. Different lines represent different local structures of fingers 1 and 2 at these specified orientations. These local zinc finger structures are taken from the original NMR structure (red), the crystal structure (blue), the joint dipole-refined structure (solid-green), or the individual dipole-refined structures (dashed-green). The orientations of the ensembles of the original structures and dipolar coupling refined structures were projected onto the axis of rotation; these ranges are shown as red stars (original NMR structures) and green X's (joint dipole-refined structures).

Dipolar coupling data for finger–finger orientation

To evaluate the sensitivity of residual dipolar couplings to the relative orientation of the zinc finger domains, the agreement between calculated and experimental dipolar coupling data was examined at different relative orientations for fingers 1 and 2. For a well-ordered structure with correctly oriented domains, the agreement between calculated and experimental dipolar coupling data should be the same when fitting each

zinc finger individually as when fitting all zinc fingers together (Prestegard, 1998). However, when the fingers are oriented incorrectly with respect to each other, the optimized alignment tensors for the individual fingers are no longer the same, and one should expect a decreased agreement with experiment when fitting all fingers simultaneously. To assess the sensitivity of the method, we have optimized the alignment tensor for zinc fingers 1 and 2 for a family of different relative orientations. These were generated by fixing zinc finger 2 and rotating zinc finger 1 about various axes of rotation. This allows us to address the question of how 'incorrect' the relative orientations have to be in order to be detected by dipolar coupling data; in other words, with what range of uncertainty can we determine the relative orientations of two domains using residual dipolar couplings?

First, a rotation axis was chosen that relates the orientation between fingers 1 and 2 in the original NMR structure to that of the crystal structure. As mentioned above, this orientation is one of the most prominent differences between the NMR and the crystal structures (Figure 5). Figure 6 shows a plot of the correlation coefficient and rms error between calculated and experimental dipolar coupling data for fingers 1 and 2, when finger 1 is rotated about an axis that relates the original NMR structure to the crystal structure. The NMR orientation is at 0° rotation, as indicated by the red vertical line. A 31.9° rotation from the NMR orientation results in the crystal orientation, as indicated by the blue vertical line. The behavior of different zinc finger substructures (original NMR, crystal, joint refinement and individually refined) along this path of orientations is plotted on the same graph. This was achieved by superimposing the individual zinc finger domains of the original NMR and the crystal structures onto the overall dipolar coupling refined structure, such that the final structures have the same relative orientations between finger 1 and finger 2 but differ in the fine details of each zinc finger substructure. Also shown as red and green crosses in Figure 6 is the range of orientations adopted by the ensembles of structures for the original NMR and the joint dipolar-refined structures.

Both the original NMR and the X-ray substructures (red and blue lines in Figure 6) give a relatively flat surface along this chosen axis of rotation, with maximum correlations and minimum rms errors near the orientation of the crystal structure. Using the zinc fingers of the joint refinement (green line) or the individual finger refinement (dashed green line) produced

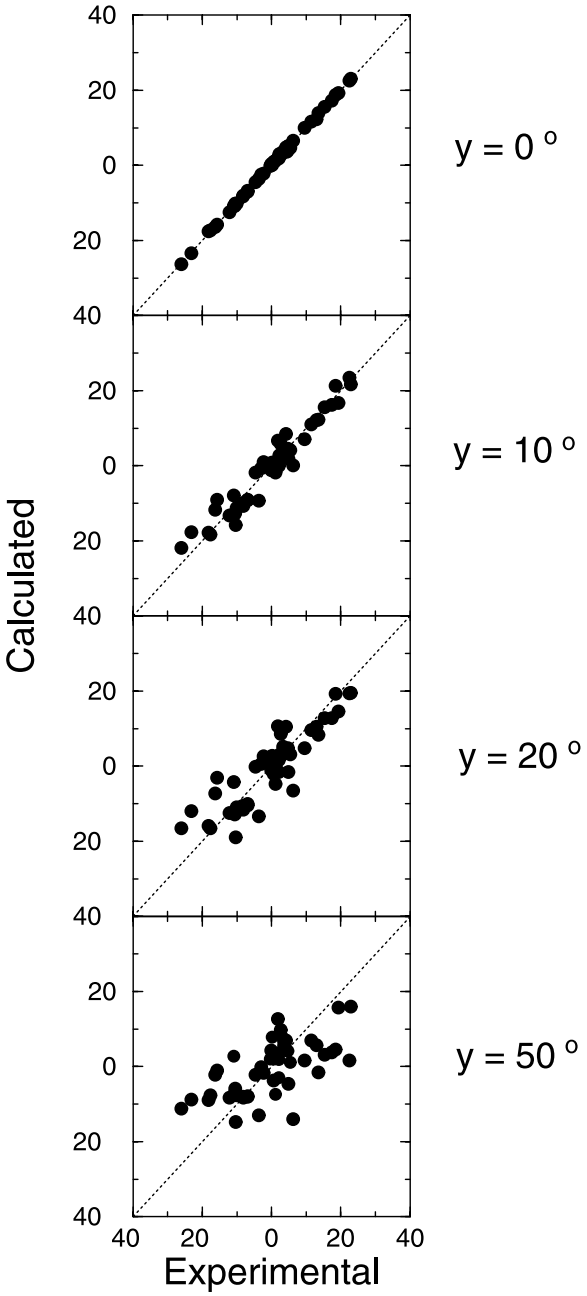

Figure 7. Plot of calculated versus experimental dipolar coupling splittings for zinc fingers 1 and 2 at different orientations of these two fingers. These are plotted for the dipolar coupling refined structure for rotations of finger 1 about an arbitrary axis, with a rotation angle of zero as the original orientation adopted in the dipolar coupling refined structure. Rotation angles (from the top): 0°, 10°, 20°, 50°. Dipolar coupling splittings are expressed in Hz, and show only data from the core regions of fingers 1 and 2. The original NMR structure and the dipolar coupling refined structure are taken from the structure in the family closest to the mean.

a different behavior. Here, the best agreement between calculated and experimental data seems to lie between the NMR and the crystal orientations. Furthermore, the range covered by the family of joint dipolar-refined structures is smaller (8.9°) than that of the original structures (24.3°), indicating that the joint dipole-refined structures adopt more well-defined interdomain orientations. The peak (or dip) in Figure 6 is much sharper for the structures that include dipolar coupling restraints (either for the whole structure, or for each finger individually). This shows that the better the domain substructures fit the local dipolar data, the more precisely can one determine interdomain orientations. The optimal orientation using the individually refined fingers (dashed green line in Figure 6) closely matches that found when all constraints are included (green line), within the range of about 10° seen in the family (green crosses).

Figure 7 shows another way of visualizing the progressively poorer agreement with experimental dipolar coupling data as the structure adopts less correct finger–finger orientations. The top plot represents the dipolar-refined structure, and subsequent plots represent increased rotation about an arbitrary axis of zinc finger 1, holding finger 2 fixed. The calculated versus experimental dipolar splittings lie on a straight line at the starting orientation, consistent with the high correlation and low rms error shown in Figure 6. As we rotate zinc finger 1 further from the optimal orientation, the points become more scattered. For many structures which have not been refined against dipolar coupling data, the agreement between calculated and experimental data might resemble that of the second plot in Figure 7. In such a case, one could still distinguish correct orientations from incorrect ones, but with less precision. Hence, residual dipolar splittings are useful for examining interdomain orientations, but the range of uncertainty depends on how well the individual domain substructures agree with the dipolar coupling data. The amount of uncertainty can be qualitatively determined by the sharpness of the maximum correlation peak when the correlation is plotted for different interdomain orientations, as in Figure 6.

Conclusions

The use of residual dipolar coupling constants for structure refinement holds great promise for improving the quality of NMR structures. Dipolar couplings can provide long-range structural information to supplement the traditional short-ranged NMR restraints. Two caveats have emerged from the present studies.

First, when using dipolar splittings as restraints, one must avoid distorting the local structure in order to fit the dipolar coupling data. In our dipolar coupling refinement of the TFIIIA-DNA complex, we have increased weights on dihedral angle restraints and included additional angle restraints to overcome this problem. Use of as small a value of $k_{dipolar}$ as possible is also helpful. Second, the local structure of each domain plays an important role in assessing the relative orientation between domains. The better the agreement of the local structure with dipolar coupling data, the more precisely one can determine relative orientations. The intradomain structure affects not only the range of orientational uncertainty, but can also affect which orientation is considered optimal (Figure 6). Therefore, care must be taken in the interpretation of results. In the present case, for example, the use of dipolar restraints alone (in conjunction with either the X-ray or original NMR structures of the individual fingers) would allow only a relatively imprecise assessment of the interdomain orientation (see the red and blue lines in Figure 6). When the dipolar results are used in combination with NOE restraints and torsion restrictions based on coupling constants (as in the green lines in Figure 6), the structural precision becomes greater.

An alternative approach to the analysis of domain orientation has been considered by Prestegard and coworkers (Fischer et al., 1999; Losonczi et al., 1999). This uses singular value decomposition to determine alignment tensors that best describe dipolar coupling data, and (unlike the present analysis) provides estimates of the uncertainties in the principal directions of the fitted alignment tensors. The key to both methods lies in comparisons between results using one domain at a time to results using data for the whole system, but the SVD method may be particularly helpful for generating an initial orientational model.

This study has resulted in an improved set of structures of the TFIIIA-DNA complex, refined with dipolar coupling restraints in addition to the original distance and torsion restraints. The new structures are similar in their overall features to the original NMR structures, with a heavy-atom rmsd of 0.4 Å between the mean structures of the new and original families. The most prominent difference stems from the increased preciseness and accuracy in defining relative orientations between zinc finger domains upon the addition of dipolar restraints, illustrating the utility of

residual dipolar coupling data for determining long-range interactions. However, since variations in the details of the local domain structures limit the precision of the interdomain orientations, care must be taken in interpreting the results. Further analysis of the structures, including a description of hydration at the protein–DNA interface, will be presented elsewhere.

Acknowledgements

This work was supported by NIH grants GM45811 (D.A.C.) and GM36643 (P.E.W.). V.T. was supported by a pre-doctoral fellowship from the La Jolla Interfaces in Science program. T.-H.H. was supported by a grant from the National Science Council, Republic of China (NSC88-2113-M-001-044). We thank Jim Prestegard for helpful discussions.

References

Banci, L., Bertini, I., Huber, J.G., Luchinat, C. and Rosato, A. (1998) *J. Am. Chem. Soc.*, **120**, 12903–12909.

Bastiaan, E.W., MacLean, C., van Zijl, P.C.M. and Bothner-By, A.A. (1987) *Annu. Rep. NMR Spectrosc.*, **19**, 35–77.

Biedenharn, L.C. (1960) In *Nuclear Spectroscopy, Part B* (Ed. F. Azjenberg-Selove), Academic Press, New York, NY, p. 732.

Bothner-By, A.A. (1996) In *Encyclopedia of Nuclear Magnetic Resonance* (Eds. D.M. Grant and R.K. Harris), John Wiley, London, pp. 2932–2938.

Brüschweiler, R., Liao, X. and Wright, P.E. (1995) *Science*, **268**, 886–889.

Case, D.A., Pearlman, D.A., Caldwell III, J.C., Cheatham, T.E., Ross, W.S., Simmerling, C.L., Darden, T.A., Merz, K.M., Stanton, R.V., Cheng, A.L., Vincent, J.J., Crowley, M., Ferguson, D.M., Radmer, R.J., Seibel, G.L., Singh, U.C., Weiner, P.K. and Kollman, P.A. (1997) *AMBER 5*, University of California, San Francisco, CA.

Cavanagh, J., Fairbrother, W.J., Palmer III, A.G. and Skelton, N.J. (1996) *Protein NMR Spectroscopy. Principles and Practice*, Academic Press, San Diego, CA.

Clore, G.M. and Gronenborn, A.M. (1998) *Proc. Natl. Acad. Sci. USA*, **95**, 5891–5898.

Clore, G.M., Starich, M.R., Bewley, C.A., Cai, M. and Kuszewski, J. (1999) *J. Am. Chem. Soc.*, **121**, 6513–6514.

Fischer, M.W.F., Losonczi, J.A., Weaver, J.L. and Prestegard, J.H. (1999) *Biochemistry*, **38**, 9013–9022.

Foster, M.P., Wuttke, D.S., Radhakrishnan, I., Case, D.A., Gottesfeld, J.M. and Wright, P.E. (1997) *Nat. Struct. Biol.*, **4**, 605–608.

Lipari, G. and Szabo, A. (1982) *J. Am. Chem. Soc.*, **104**, 4546–4559.

Losonczi, J.A., Andrec, M., Fischer, M.W.F. and Prestegard, J.H. (1999) *J. Magn. Reson.*, **138**, 334–342.

Nolte, R.T., Conlin, R.M., Harrison, S.C. and Brown, R.S. (1998) *Proc. Natl. Acad. Sci. USA*, **95**, 2938–2943.

Ottiger, M., Delaglio, F. and Bax, A. (1998a) *J. Magn. Reson.*, **131**, 373–378.

Ottiger, M., Delaglio, F., Marquardt, J.L., Tjandra, N. and Bax, A. (1998b) *J. Magn. Reson.*, **134**, 365–369.

Prestegard, J.H. (1998) *Nat. Struct. Biol.*, **5**, 517–522.

Tjandra, N. and Bax, A. (1997) *Science*, **278**, 1111–1114.

Tjandra, N., Omichinski, J.G., Gronenborn, A.M., Clore, G.M. and Bax, A. (1997) *Nat. Struct. Biol.*, **4**, 732–737.

Tolman, J.R., Flanagan, J.M., Kennedy, M.A. and Prestegard, J.H. (1997) *Nat. Struct. Biol.*, **5**, 292–297.

Wuttke, D.S., Foster, M.P., Case, D.A., Gottesfeld, J.M. and Wright, P.E. (1997) *J. Mol. Biol.*, **273**, 183–206.

Appendix

The coordinate transformations illustrated in Equations 1 to 3 are a common feature of many analyses of dipolar coupling tensors in oriented media. Here we outline a derivation of Equation 3, which connects the tensor described in terms of the *instantaneous* bond vectors to one that is defined in terms of the *average* bond vector. Following the notation in the main body of the text, Γ_{pq} is defined as

$$\Gamma_{pq} = \left\langle \frac{3}{2}(\hat{p}\cdot\hat{z}'')(\hat{q}\cdot\hat{z}'') - \frac{1}{2}\delta_{pq} \right\rangle \tag{A1}$$

If we now introduce new axes *r* and *s*, whose *z* axis is along the average bond direction $\hat{z}^{av}$, the Γ_{pq} can be expressed in this new coordinate frame:

$$\Gamma_{pq} = \sum_{r,s} \left\langle (\hat{z}''\cdot\hat{r})(\hat{z}''\cdot\hat{s}'') \left[\frac{3}{2}(\hat{p}\cdot\hat{r})(\hat{q}\cdot\hat{s}) - \frac{1}{2}\delta_{pq} \right] \right\rangle \tag{A2}$$

The final term in square brackets involves angles between the overall molecular axes $(\hat{p}, \hat{q})$ and the axes of the average bond vector angles $(\hat{r}, \hat{s})$; these angles are independent of molecular motion, and hence can be taken outside of the averaging brackets. We can also take advantage of the fact that $(3ab - \delta_{ab})$ is a traceless quantity to rewrite this:

$$\Gamma_{pq} = \frac{2}{3}\sum_{r,s} \left\langle \frac{3}{2}(\hat{z}''\cdot\hat{r})(\hat{z}''\cdot\hat{s}'') - \frac{1}{2}\delta_{rs} \right\rangle \left[\frac{3}{2}(\hat{p}\cdot\hat{r})(\hat{q}\cdot\hat{s}) - \frac{1}{2}\delta_{pq} \right] \tag{A3}$$

Now, if the motion of the instantaneous bond vector $\hat{z}''$ about its average position $\hat{z}^{av}$ is cylindrically symmetric, then the first term in brackets in Equation A3 will be a diagonal tensor, whose *zz* component is

$$S \equiv \left\langle \frac{3}{2}(\hat{z}''\cdot\hat{z}^{av})^2 - \frac{1}{2} \right\rangle \tag{A4}$$

and whose *xx* and *yy* components are each $-S/2$. Direct substitution of these values into Equation A3 and re-arrangement yields Equation 3. An elegant discussion of these types of transformations is given by Biedhenharn (1960).

The original Lipari–Szabo (1982) analysis is generally represented in terms of an order parameter determined from the contribution of internal motion to the correlation function:

$$C(\tau) \equiv \left\langle \frac{3}{2}(\hat{z}''(0) \cdot \hat{z}''(\tau)) - \frac{1}{2} \right\rangle \tag{A5}$$

This is evaluated at a time τ where $C(\tau)$ reaches a plateau and becomes approximately independent of τ. Using the same sort of algebra to carry out the cylindrical averaging of $\hat{z}''$ about $\hat{z}^{av}$ yields:

$$\begin{aligned} C(\tau) &= \left\langle \frac{3}{2}(\hat{z}''(0) \cdot \hat{z}^{av}) - \frac{1}{2} \right\rangle \left\langle \frac{3}{2}(\hat{z}^{av} \cdot \hat{z}''(\tau)) - \frac{1}{2} \right\rangle \\ &= S^2 \end{aligned} \tag{A6}$$

This demonstrates that the definition of S in Equation 3 is formally equivalent to that of the usual Lipari–Szabo approach. It should be noted, however, that the time τ of the plateau in the internal motional correlation function $C(\tau)$ must be shorter than the rotational correlation time for the conventional Lipari–Szabo analysis of dipolar relaxation, whereas the influence of internal motion on direct dipolar couplings is not subject to this limitation. In principle, this offers an approach to detection of longer time scale motions by NMR (Tolman et al., 1997). The appearance of a simple scalar order parameter in Equation 3 follows from the assumption of cylindrical symmetry in the motional averaging of the instantaneous bond vector about its average position. For more complex motions, the 'order parameter' would itself become a tensor. The present result is a generalization of the diffusion-in-a-cone model previously considered by Tolman et al. (1997), which also has cylindrical symmetry. It would be, of course, possible to characterize the internal motion with a more complex model, but such experimental characterizations are only available for a few proteins, whereas Lipari–Szabo order parameters derived from ^{15}N relaxation measurements have been widely reported.